

FOREST CANOPY WAVES: THE LONG-WAVELENGTH COMPONENT

MANUEL PULIDO¹ and GEORGE CHIMONAS^{2,*}

¹*Grupo de Física de la Atmosfera, FaMAF, Universidad Nacional de Córdoba, Argentina;* ²*School of Earth and Atmospheric Sciences, Georgia Institute of Technology, Atlanta, GA 30332-0340, U.S.A.*

(Received in final form 2 January 2001)

Abstract. Air flowing over a forest canopy is examined for instabilities driven by Jeffreys' drag mechanism. The calculations indicate that the mechanism is generally effective in strong wind conditions and extremely effective when the boundary layer supports wave trapping. The instability forces the free wind down amongst the trees, creating episodes of stress in the foliage.

Keywords: Canopy waves, Gusts, Instability, Turbulence.

1. Introduction

Flows may have instabilities that grow by modulating frictional stresses, as Jeffreys demonstrated for water running down a rough inclined channel (Jeffreys, 1925). A similar drag mechanism destabilizes the Earth's surface wind (Chimonas, 1993), while this paper applies the mechanism to the wind over a forest canopy. In a forest, a wave forces the free-air stream down into the trees creating a drag, and this drag feeds back into the wave – the feedback causes the wave to amplify. The instability becomes more effective as the speed of the free wind increases and most effective when there is a shallow near-surface wave duct.

This study is intended to demonstrate the new application of Jeffreys' drag mechanism and generate interest in it as an integral part of boundary-layer dynamics. At this time the only concise formulation of the mechanism involves a long-wavelength approximation, and our results demonstrate that the canopy-drag instability is effective in this limit. However, the long-wave formulation predicts a monotonic increase in growth rate as the wavelength decreases, which is almost certainly incorrect; thus the scale at which the instability peaks is currently unknown, inviting work that treats the smaller scales consistently.

Observations of waves and eddies in a canopy are reviewed by Raupach et al. (1996). The review is mainly concerned with the small-scale structure, and Raupach et al. show that this end of the spectrum obeys Kelvin–Helmholtz scaling laws. Raupach et al. (1996) also identify a long-wavelength component that modulates the short-wavelength activity, and refer to this long-wavelength component

* Corresponding author: George Chimonas, E-mail: george.chimonas@eas.gatech.edu



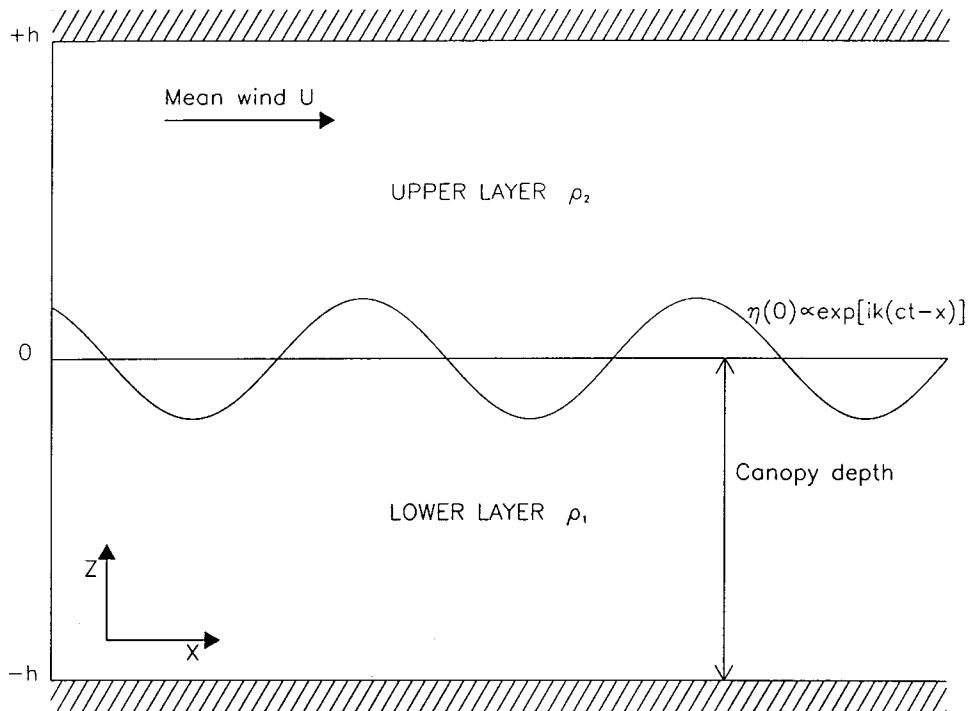


Figure 1. The structure of the two-layer model. The flow is ducted between rigid plates at $z = \pm h$.

as ‘inactive turbulence’, which is generally visualized in terms of large vortices. However, inactive turbulence includes a wave component – Einaudi and Finnigan (1993) postulate a continuous exchange between waves and turbulence at these scales – and our study shows that Jeffreys’ mechanism is a very effective source of long-wavelength boundary-layer waves, and thus a source for the long-wavelength disturbances in all their forms. We suspect that Jeffreys’ mechanism also enhances the growth of the smaller-scale Kelvin–Helmholtz disturbances, although confirmation of this (or its rejection) must await a short-wavelength formulation of the mechanism.

2. A Two-Layer Demonstration

The instability is demonstrated with the simplest model that incorporates Jeffreys’ mechanism into canopy drag. The undisturbed flow, shown in Figure 1, consists of two homogeneous layers of incompressible fluid each filling half the space between rigid horizontal plates set $2h$ apart. The lower layer is at rest and has density ρ_1 , while the upper layer has horizontal speed U and density ρ_2 . The lower half of the space contains trees that create a drag on any flow within them.

Coordinates are chosen with x parallel to the mean wind and z in the vertical direction, while t denotes time. A wave with phase speed c and wavenumber k propagates along the layers causing a vertical displacement η' of fluid parcels about their mean heights

$$\eta'(x, t) = \eta(z) \exp ik(ct - x). \quad (1)$$

The displacement brings the air above into contact with the trees, and the friction-force per unit volume exchanged between wind and foliage is formulated with the aerodynamic law

$$\mathbf{F}(x, z, t) = -\rho(C/h)\mathbf{V}|\mathbf{V}|, \quad (2)$$

where \mathbf{V} is the air velocity through the foliage and C/h is an effective volume-drag coefficient (C is a dimensionless number and h , the canopy depth, is set equal to the depth of the lower layer). The resistance exerted by a canopy is a function of many variables, including the aerodynamic drag coefficients of the trunks, branches and leaves, and the cross sections and volume-densities of these elements (Amiro, 1990). The formulation (2) provides the overall friction so the C used here is a combination of the factors presented in Amiro (1990).

As shown in Figure 1, a sub-layer of depth $\eta(0)$ is forced below $z = 0$ so that the half-cycles with $\eta'(x, 0, t) < 0$ are brought within the trees. Then, to first-order in the wave amplitude, the total friction force acting on a vertical column of unit cross-section drawn through the upper fluid is

$$\int_{\text{upper-layer fluid}} \mathbf{F}(x, z, t) dz = \begin{cases} -\hat{\mathbf{x}}\rho(C/h)U^2|\eta'(x, 0, t)| & \text{for } \eta'(x, 0, t) < 0 \\ 0 & \text{for } \eta'(x, 0, t) > 0, \end{cases} \quad (3)$$

where $\hat{\mathbf{x}}$ is the unit vector in the direction of the mean wind. Since the lower fluid is at rest there is no first-order drag on it; if the lower fluid contained a mean wind it would experience a stabilizing first-order drag (Lee, 1997).

Following the spirit of Jeffreys' (1925) approach two simplifying approximations are made: the wavelength is taken to be greater than $2\pi h$ (so that $(kh)^2 < 1$), and the force (3) is redistributed uniformly over the upper-layer column (presumably by turbulence). The phase speed c of the wave then obeys the dispersion relation (see Appendix A)

$$c^2 + (c - U)^2 - g \frac{\Delta\rho}{\rho} h - i \frac{CU^2}{2kh} = 0, \quad (4)$$

where $\Delta\rho = (\rho_1 - \rho_2)$ is the density drop between the layers and ρ is the average density. Only the stable stratification $\Delta\rho > 0$ is considered.

When the drag is omitted the solutions of (4) reduce to the bounded two-layer, long-wavelength, Kelvin-Helmholtz result

$$c = \frac{U}{2} \pm \sqrt{\frac{hg \Delta\rho}{2\rho} - \frac{U^2}{4}}. \quad (5)$$

There is no instability (c is real) if the energy tied up in the stable-stratification $gh \Delta\rho$ exceeds the kinetic energy $\frac{1}{2}\rho U^2$. But with the drag included (4) always has an unstable root (imaginary part of $c < 0$). The limiting condition for Kelvin–Helmholtz waves, $gh \Delta\rho/2\rho - U^2/4 = 0$, is particularly easy to examine. The frictionless solution (5) reduces to a single, non-growing wave propagating at the mean speed $U/2$ of the fluid, while with friction there are two solutions of (4), one that grows in time and one that decays

$$c = \frac{U}{2} \left(1 \pm (1 + i) \sqrt{\frac{C}{2kh}} \right). \quad (6)$$

The growing mode (the one with the negative imaginary part) travels more slowly than the mean fluid speed $U/2$ while the decaying mode is faster. The growing mode has the following properties:

- (a) As its wavelength $2\pi/k$ increases the wave becomes more retrograde relative to the mean flow, eventually moving in the opposite direction to the wind. The instability then has no critical level. Jeffreys' water-channel instabilities also lacked critical levels, and this is a feature that distinguishes drag instabilities from shear instabilities as the latter always have critical levels.
- (b) The wave (1) grows exponentially at the rate $-k\text{Im}[c]$, which equals $U/2\sqrt{Ck/2h}$, so the growth rate is zero for infinite wavelength and increases continuously towards shorter wavelengths. Since the formulation has used the long-wavelength approximation $(kh)^2 < 1$ its predictions are already questionable at $(kh)^2 = 1$ and we do not know where the instability maximizes.
- (c) The growth rate increases with the strength of the free wind U . This is expected, since the wind is the sole source of energy. But it also suggests that instability and hence gusting should be more common in strong-wind conditions.
- (d) The growth rate increases with the coefficient C , which emphasizes that friction is creating the instability. Lee and Barr (1998), observed that wave activity in a forest does indeed decrease with leaf-fall and its attendant reduction of C .

A numerical example gives a sense of the strength of these instabilities. The time τ for a wave to grow by one factor of e is $1/(\text{Imaginary part of } ck)$, so from (b) $\tau = 2/U\sqrt{2h/Ck}$. Setting $U = 5 \text{ m s}^{-1}$, $h = 15 \text{ m}$, $C = 1.5$ (the large end of observed values) and a wavelength of 100 m ($kh \approx 1$) leads to $\tau = 7 \text{ s}$. Even wavelengths of 1 kilometre ($kh \approx 0.1$) take only 23 s to exponentiate, and thus have explosive growth rates. The instability would still be meteorologically significant if factors not considered here reduced growth by an order of magnitude.

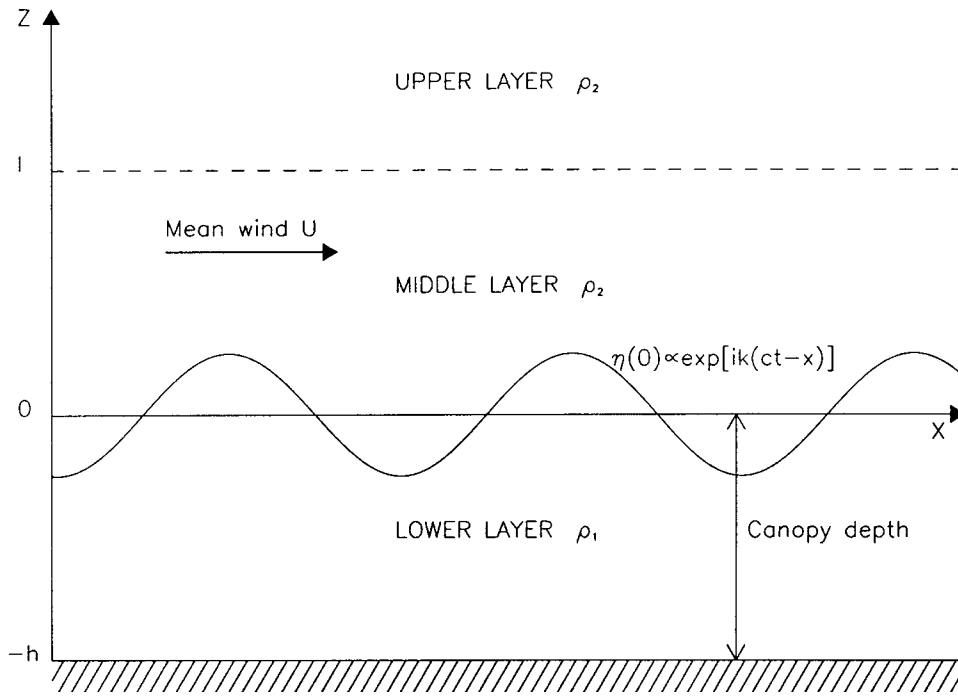


Figure 2. The structure of the three-layer model.

3. A Model without the Upper Plate

The finite duct of Section 2 is opened to the overlying atmosphere, the rigid plate is removed and the free atmosphere is continued upward to mimic a deep, neutrally stratified residual layer, Figure 2. The drag on the atmosphere that results when the wave forces the free wind down into the trees is redistributed (presumably by turbulence) over a middle-layer column of thickness l . The dispersion relation for the wave (1) in this flow is (Appendix A)

$$c^2 + (c - U)^2 \frac{kh}{(1 + kl)} - g \frac{\Delta\rho}{\rho} h - i \frac{CU^2}{2(1 + kl)} = 0. \tag{7}$$

The long-wavelength approximation $(kh)^2 < 1$ and the shallow-mixing approximation $(kh)^2 < 1$ are both imposed. With $(kl)^2 \ll 1$ the value of l has no significant influence in (7).

As in Section 2 the drag instability is evaluated relative to the Kelvin–Helmholtz instability. When the drag term is discarded (7) provides the Kelvin–Helmholtz solutions

$$c = U \frac{kh}{1 + k(l + h)} - \sqrt{\frac{\Delta\rho}{2\rho} \frac{gh(1 + kl)}{1 + k(l + h)} + \left(\frac{khU}{1 + k(l + h)}\right)^2 - \frac{khU^2}{1 + k(l + h)}}. \quad (8)$$

Comparing this with (5) shows that removing the upper plate has reduced the importance of the velocity terms in the regime $(kh)^2 < 1$ of the model. According to (8), even a minimal stable density contrast ($\Delta\rho > 0$) now makes c real at the longer wavelengths. However, when drag is retained, the dispersion relation (7) always has an unstable solution

$$c = U \frac{kh}{1 + k(l + h)} - \sqrt{\frac{\Delta\rho}{2\rho} \frac{gh(1 + kl)}{1 + k(l + h)} + \left(\frac{khU}{1 + k(l + h)}\right)^2 - \frac{khU^2}{1 + k(l + h)} + i \frac{CU^2}{4(1 + kl)}}. \quad (9)$$

(with the square root defined to be in the upper-half plane).

The instability retains the general properties outlined in Section 2: it is retrograde with respect to the mean flow and its growth increases with the strength of the free wind U and the coefficient C . The growth rate $-\text{Im}(ck)$ decreases with large wavelength faster than before, but long wavelengths are unstable where Kelvin–Helmholtz theory would have no instabilities.

Direct comparison of the friction contributions in (7) and (4) shows that the upper plate makes the drag instability more effective. This is because removing the plate adds additional mass to the wave but does not change the net drag force. Reduced growth is most noticeable at the longest wavelengths, as these reside to a greater degree (as Ae^{-kz}) in the fluid that is exposed by removing the plate.

4. Numerical Results

The dispersion relations for c are evaluated for characteristic canopy situations. The coefficient C varies from 0.3 for a typical stand of pines to 1.5 for spruce trees (Amiro, 1990: note that this reference resolves C into more basic factors).

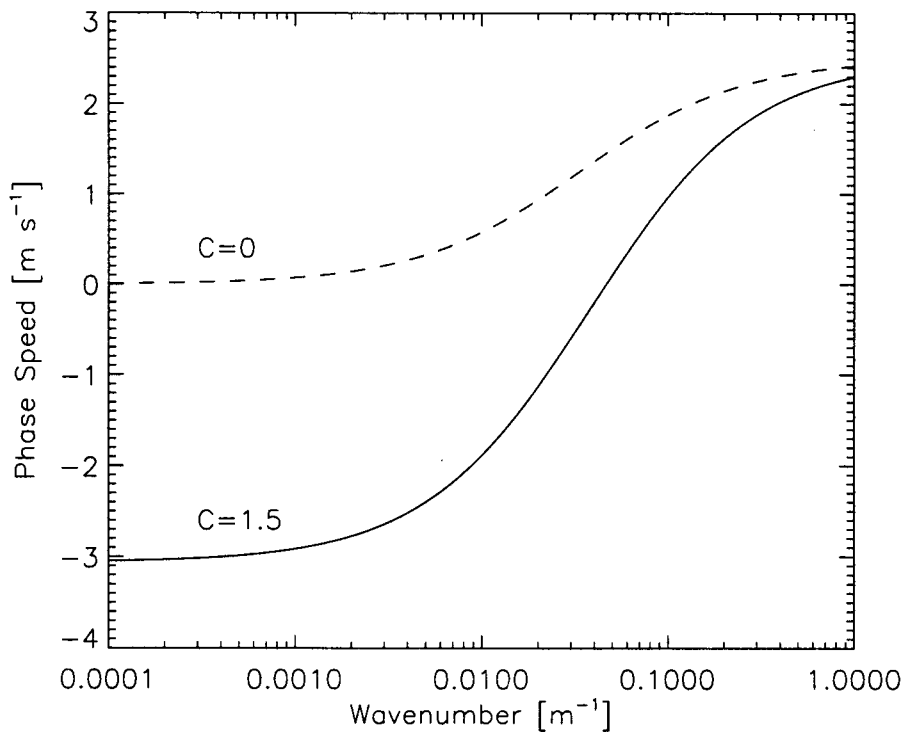


Figure 3. Wave phase speeds in the three-layer model with $\Delta\rho = 0$, $U = 5 \text{ m s}^{-1}$ and $h = l = 15 \text{ m}$.

4.1. NO UPPER PLATE, NO DENSITY CONTRAST

The governing equation is (9) with $\Delta\rho = 0$. Numerical results are given for $U = 5 \text{ m s}^{-1}$ and $h = l = 15 \text{ m}$. Figure 3 shows the phase speeds as a function of wavelength for Kelvin–Helmholtz waves ($C = 0$), and then the speeds with the large value $C = 1.5$. Figure 4 plots the time τ for a wave to grow by one factor of e ; note that the friction increases instability above the Kelvin–Helmholtz rate.

4.2. NO UPPER PLATE, STRONG STABLE DENSITY CONTRAST

As in the previous situation $U = 5 \text{ m s}^{-1}$ and $h = l = 15 \text{ m}$. The governing equation is (9) with $\Delta\rho/\rho = 0.02$; this degree of stratification, which is within the observed range (Lee, 1997; Lee et al., 1997), prevents growth of Kelvin–Helmholtz waves at the longer wavelengths. Figure 5 shows wave phase speeds for three values of the canopy friction: C set to 0, 0.3 and 1.5. Figure 6 shows the corresponding growth-times τ .

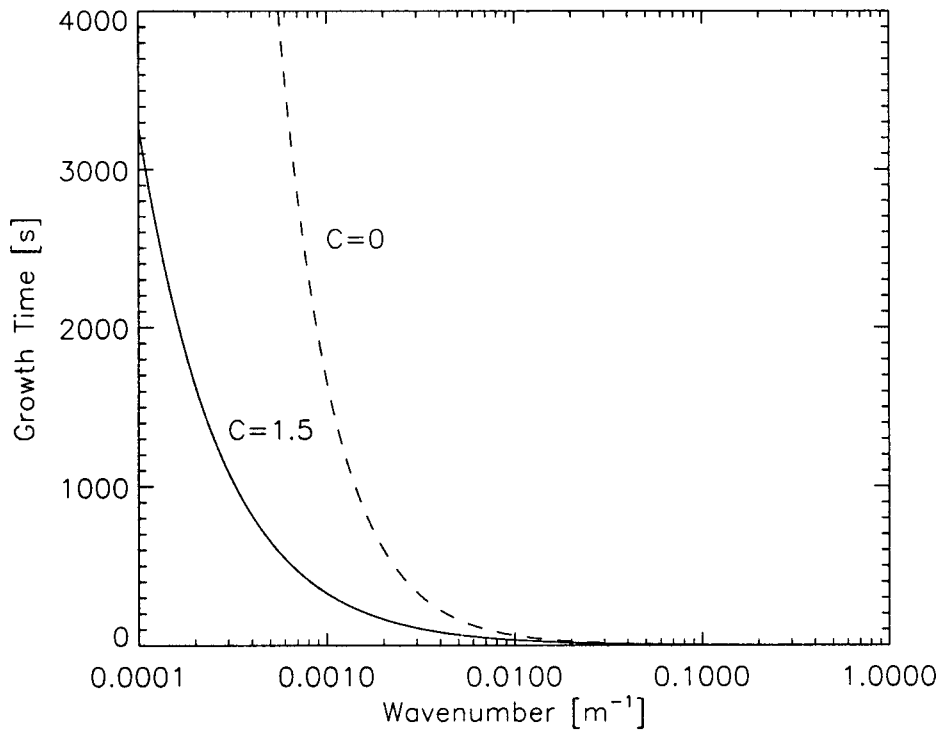


Figure 4. Time for the wave to exponentiate in the three-layer model with $\Delta\rho = 0$, $U = 5 \text{ m s}^{-1}$ and $h = l = 15 \text{ m}$.

4.3. AN UPPER PLATE AND A STRONG STABLE DENSITY CONTRAST

The governing equation is (4) with $\Delta\rho/\rho = 0.02$ and all the other parameters also the same as those used in 4.2 so that one can compare the capped and uncapped cases directly. The results, displayed in Figures 7 and 8, should be contrasted with Figures 5 and 6. The upper plate makes the instabilities an order of magnitude more effective.

5. Discussion and Conclusions

Our study indicates that Jeffreys' drag mechanism can provide useful insights into waves and eddies in a forest canopy, although the model is much too simple for realistic predictions of atmospheric behaviour. In this section we summarize the potential of the drag mechanism, we outline the developments needed to produce an acceptable atmospheric model, and we identify field observations that would help further theoretical development.

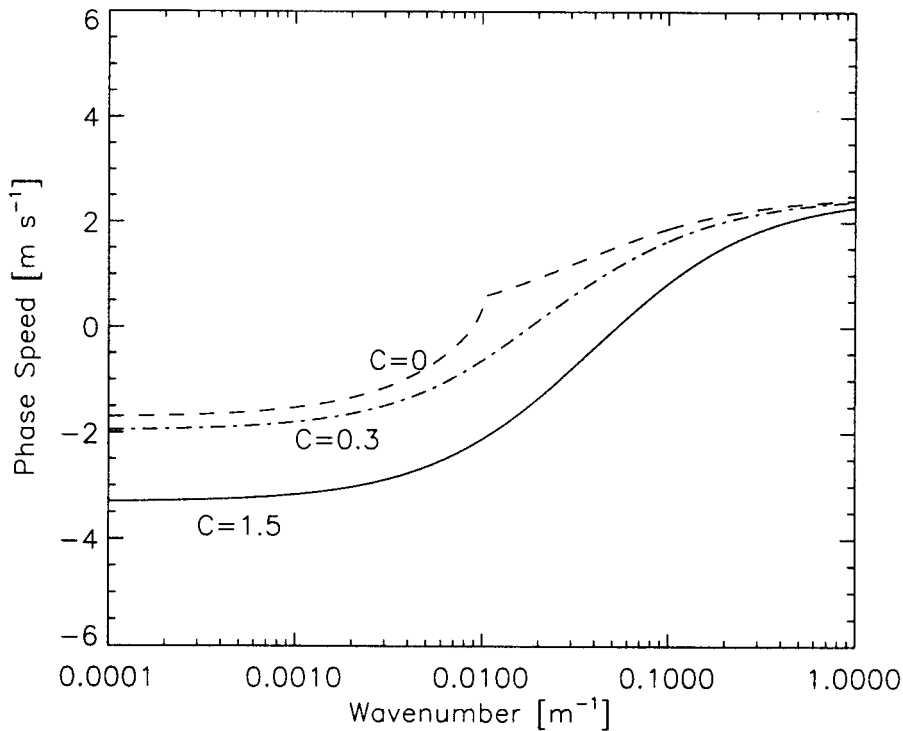


Figure 5. Wave phase speeds in the three-layer model with $\Delta\rho/\rho = 0.02$, $U = 5 \text{ m s}^{-1}$ and $h = l = 15 \text{ m}$.

5.1. POTENTIAL OF THE DRAG MECHANISM

The long-wavelength behaviour found in this study should carry over into more realistic models. Thus Figures 4, 6 and 8 show that Jeffreys' drag mechanism is more effective than the shear-instability mechanism at the longer wavelengths, a behaviour that can also be deduced from the asymptotic forms of Equations (4) and (7). Moreover, Jeffreys' mechanism can work when shear instability is suppressed by a too-stable stratification (refer to the text between Equations (5) and (6)), or the geometry of the wind profile (Section 5.3). However, it is quite possible that disturbances develop most readily when the Kelvin–Helmholtz and the Jeffreys' instabilities work together, providing a hybrid that should not be identified as one rather than the other. The suggestion by Lee et al. (1997) that the term 'canopy waves' be used to avoid presumptions about the dynamics seems appropriate.

Figures 6 and 8 also illustrate that the instabilities are much more effective when they are narrowly confined to the near-earth regions. In the model this was achieved by placing a rigid plate at the top of the boundary layer, and although rigid plates do not exist in the atmosphere over-reflecting layers can exist and can act just like perfectly reflecting plates. So complex profiles that provide wave trapping by elevated over-reflecting layers or other structures should show more long-wavelength

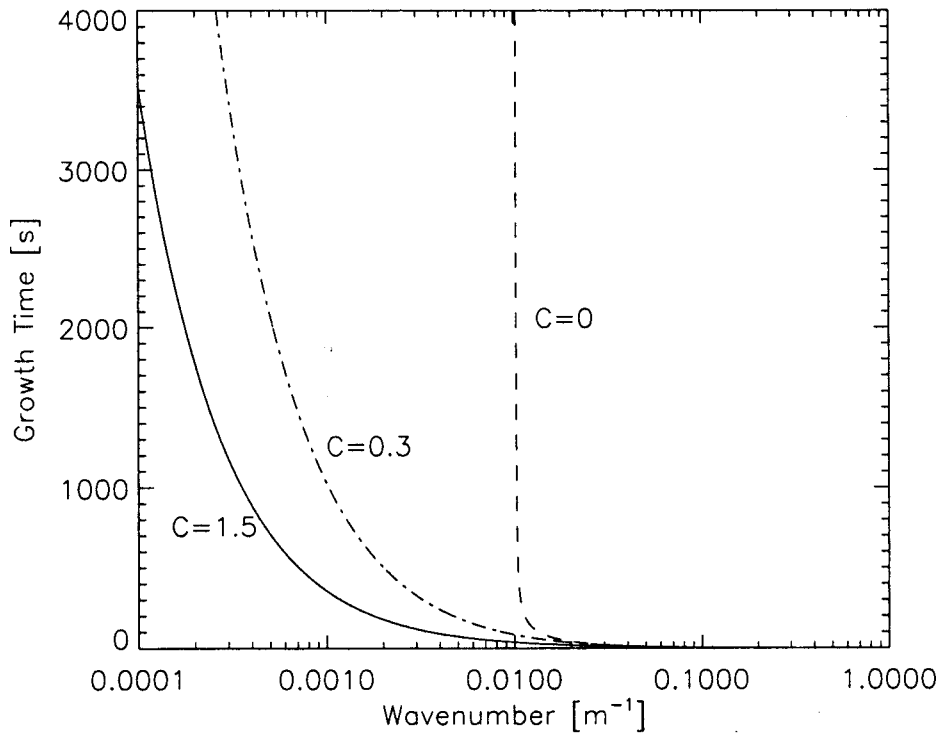


Figure 6. Time for the wave to exponentiate in the three-layer model with $\Delta\rho/\rho = 0.02$, $U = 5 \text{ m s}^{-1}$ and $h = l = 15 \text{ m}$.

gustiness than simple profiles. This enhancement applies equally to drag instabilities and shear instabilities, and it should be observable in the climatology of canopy waves.

A feature of Figures 4, 6 and 8 that is almost certainly incorrect is the ever-increasing effectiveness of the instability as its wavelength decreases. When the sudden jump of the Kelvin-Helmholtz profile is replaced by a continuous transition, the growth rates of the instabilities peak at the scale of the transition region (Miles and Howard, 1964). In addition to this transition scale, the canopy problem involves the canopy depth h and the mixing-layer depth l (introduced in Section 3). These scales will control the form of the instability at short wavelengths, and will almost certainly select a wavelength for maximum growth rate.

5.2. COMPLEXITIES THAT MUST BE ADDED TO THE MODEL

The most distressing shortcoming of the model is its use of the long-wavelength approximation, and this must be addressed to bring drag theory to a state comparable with modern shear-instability theory. This may prove difficult, since drag is at root a non-linear, turbulent problem. Jeffreys used an integral method to replace the complex spatial distribution of turbulent stresses by their net effect – the aero-

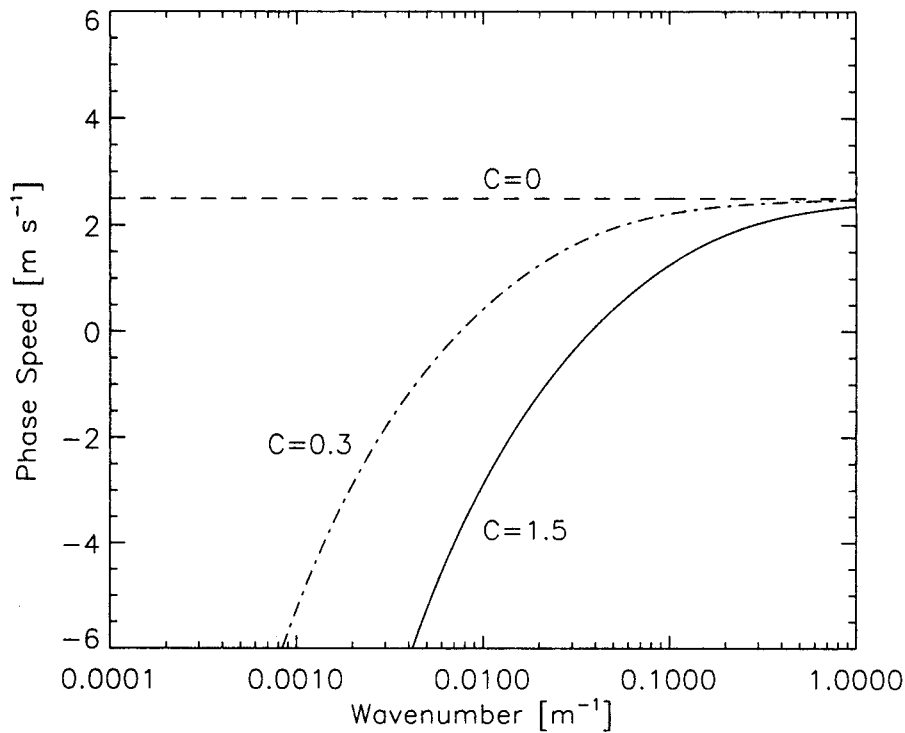


Figure 7. Wave phase speeds in the two-layer model with $\Delta\rho/\rho = 0.02$, $U = 5 \text{ m s}^{-1}$ and $h = l = 15 \text{ m}$.

dynamic drag at the surface. This provides a brilliant simplification of the problem, but it is not at all obvious how to extend the approach to short-wavelength disturbances. The alternative is a fully numerical approach, which we do not contemplate attempting. However, if a suitable linearised formulation can be developed the next step will be to contrast instabilities in log-linear wind profiles with instabilities in free-shear wind profiles. Both forms have been postulated for the structure above a canopy-and they have very different consequences for shear instabilities (Section 5.3).

5.3. POINTS FOR FIELD OBSERVATIONS

The structure of the mean boundary-layer flow provides the best clues to the origin of any waves observed there. The clearest case is provided by the neutrally-stratified state, since this is governed by Rayleigh's inflection point theorem, which may be stated as 'An inviscid, neutrally stratified flow in which the shear increases or decreases monotonically does not have any (linearized) shear instabilities'. The classical boundary-layer profiles (log and log-linear) all satisfy this condition and are thus immune from simple shear instabilities. Viscosity does allow Tollmein-Schlichting instabilities in uninflected profiles, but these are very slow-growing

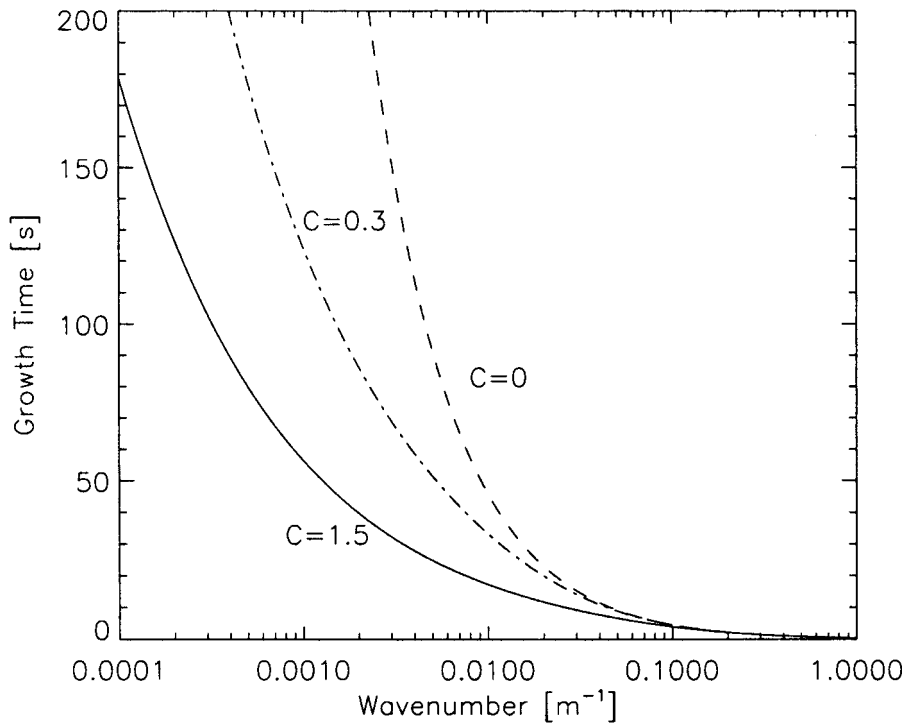


Figure 8. Time for the wave to exponentiate in the two-layer model with $\Delta\rho/\rho = 0.02$, $U = 5 \text{ m s}^{-1}$ and $h = l = 15 \text{ m}$.

(Maslowe and Thompson, 1971) and are not regarded as serious contributors to atmospheric activity.

The conventional view holds that the mean flow above a canopy obeys the log-linear law, whence Rayleigh's theorem would eliminate shear instabilities in neutral or near-neutral conditions, leaving the field to Jeffreys' mechanism or whatever new theories could be devised. But Raupach et al. (1996) propose that the flow above a canopy includes a free-shear layer with an inflection point. They provide an analysis that extracts a shear scale for this layer and they show that the observed wave spectrum is consistent with Kelvin-Helmholtz theory based on this scale.

Thus a very interesting and potentially important direction for field research would be to determine whether the flow above a forest canopy is, or is not, inflection-free. And regardless of whether it has a shear layer, an accurate form of the profile is essential to further computations of the spectrum of instabilities.

Acknowledgements

This research was supported in part by grant ATM-9422869 from the National Science Foundation and in part by CONICET and FOMEC, sponsors of Manuel Pulido's visit to the Georgia Institute of Technology.

Appendix A: Derivation of the Dispersion Relations

The unperturbed flow \mathbf{V}_0 of the model is

$$\mathbf{V}_0 = \hat{\mathbf{x}}V_0 = \begin{cases} \hat{\mathbf{x}}U & \text{above the canopy layer} \\ 0 & \text{within the canopy layer.} \end{cases} \quad (\text{A1})$$

The instabilities have the form

$$\{u, w, p, \eta\} = \{u'(z), w'(z), p'(z), \eta'(z)\} \exp ik(ct - x), \quad (\text{A2})$$

where $\{u', w'\}$ are the x and z components of the perturbation velocity, p' is the perturbation pressure and η' is the vertical displacement of the streamlines. The waves of interest have periods less than an hour so the derivations given here ignore Coriolis accelerations from the outset (we have checked for subtle influences of the Coriolis terms and have found none). Following Jeffreys' original study, the long-wavelength approximation is invoked: $u'(z)$ and $p'(z)$ are set constant within each layer of the two-layer model and within each of the two lower layers of the three-layer model.

The perturbed atmosphere is treated as in an ideal, incompressible fluid that exchanges momentum with the tree canopy through aerodynamic drag. The incompressibility condition applied to the wave (A2) produces

$$\frac{\partial w'}{\partial z} = ik u'. \quad (\text{A3})$$

Within a layer where $u'(z) = u_{\text{layer}}$ is a constant the integration of (A3) leads to

$$w'(z) = a + (iku_{\text{layer}})z, \quad (\text{A4})$$

where the constant a must be determined by a boundary condition.

Within each layer the linearized x -component of the momentum equation reduces to

$$\rho \left(\frac{\partial}{\partial t} + V_0 \frac{\partial}{\partial x} \right) u' = -\frac{\partial p'}{\partial x} + \mathbf{F}'_x \quad (\text{A5})$$

hence

$$\rho i(c - V_0)ku' = ikp' + \mathbf{F}'_x. \quad (\text{A6})$$

The term \mathbf{F}'_x is the wave component of the drag force (2) introduced when the mean wind (10) is drawn down into the tree canopy. The column integral of the drag force is given by (3), and the component $\exp ik(ct - x)$ is extracted by Fourier theory as

$$\int_{\text{layer}} \mathbf{F}'_x dz = \begin{cases} \frac{1}{2}\rho_2(C/h)U^2\eta'(x, 0, t) & \text{for the layer forced down into the canopy} \\ 0 & \text{for all other layers.} \end{cases} \quad (\text{A7})$$

The result (A7) is only correct for linear theory.

Integrating (A6) over the layer-depth L and using (A7) gives the long-wavelength approximation

$$\rho_2 i(c - U)ku_2 L_2 = ikL_2 p_2 + \frac{1}{2}\rho_2(C/h)U^2\eta(0), \quad (\text{A8})$$

for the upper layer of the two-layer model (Figure 1, and $L_2 = h$) and the middle layer of the three-layer model (Figure 2, and $L_2 = l$). There is no drag term in the lowest layer and (A6) gives directly

$$\rho_1 cu_1 = p_1. \quad (\text{A9})$$

DISPERSION RELATION FOR THE TWO-LAYER MODEL

The two-layer model is bounded by rigid plates at $z = \pm h$, so $w'(z)$ must be zero at these points and (A4) yields

$$w'(z) = \begin{cases} iku_2(z - h) & \text{upper layer} \\ iku_1(z + h) & \text{lower layer.} \end{cases} \quad (\text{A10})$$

The displacement $\eta = w'(z)/ik(c - V_0)$ must be continuous across the interface of the two layers, hence

$$\frac{-hu_2}{(c - U)} = \frac{hu_1}{c}. \quad (\text{A11})$$

The pressure must also be continuous across the displaced interface, so from (A8), (A9) and the hydrostatic condition of the mean state

$$\rho_2(c - U)u_2 + \left[\frac{i}{2kh}\rho_2(C/h)U^2 - \rho_2 g \right] \frac{hu_1}{c} = \rho_1 cu_1 - \rho_1 g \frac{hu_1}{c}. \quad (\text{A12})$$

The condition that (A11) and (A12) have a nontrivial solution provides the dispersion relation

$$(c - U)^2 + \frac{\rho_1}{\rho_2}c^2 - \frac{(\rho_1 - \rho_2)}{\rho_2}gh - \frac{i}{2kh}CU^2 = 0. \quad (\text{A13})$$

Since atmospheric inversions are in the regime $\rho_1 = \rho_2 + \Delta\rho$ with $\Delta\rho/\rho_2 \ll 1$ the densities of the layers can be set equal to their mean except in the difference term to give the form (4) presented in the text.

DISPERSION RELATION FOR THE THREE-LAYER MODEL

The three-layer model builds on the two-layer model, replacing the upper plate with an unbounded homogeneous flow. In this uppermost region the disturbance is the bounded solution

$$\{u, w, p, \eta\} = u_3 \left\{ 1, -i, \rho_2(c - U), \frac{-1}{(c - U)k} \right\} \exp[ik(ct - x) - kz]. \quad (\text{A14})$$

In the middle layer, which has depth l , (A4) and (A8) become

$$\left. \begin{aligned} \rho_2 i(c - U)ku_2 l &= iklp_2 + \frac{1}{2}\rho_2(C/h)U^2\eta(0) \\ w'(z) &= w'(l) + iku_2(z - l). \end{aligned} \right\} \quad (\text{A15})$$

Continuity of pressure and displacement at $z = l$ relates the fields (A14) and (A15), requiring that

$$iw'(l)\rho_2(c - U) = p_2. \quad (\text{A16})$$

The lowest layer still obeys (A9) and (A10)

$$\left. \begin{aligned} \rho_1 cu_1 &= p_1 \\ w'(z) &= iku_1(z + h) \end{aligned} \right\} \quad (\text{A17})$$

and continuity of pressure and displacement at the displaced interface of the lower two layers requires

$$\eta(0) = \frac{w'(l) - iku_2 l}{ik(c - U)} = \frac{u_1 h}{c} \quad (\text{A18})$$

and

$$iw'(l)\rho_2(c - U) = \left[\rho_1 c - \frac{h}{c}g(\rho_1 - \rho_2) \right] u_{11}. \quad (\text{A19})$$

The condition that (A15) through (A19) have a nontrivial solution provides the dispersion relation. In the approximation that $\rho_1 = \rho_2 + \Delta\rho$ with $\Delta\rho/\rho_2 \ll 1$ the densities of the layers can be set equal to their mean except in the gravitational term to yield the result (7) presented in the text.

References

- Amiro, B.: 1990, 'Drag Coefficients and Turbulence Spectra within Three Boreal Forest Canopies', *Boundary-Layer Meteorol.* **52**, 227–246.

- Chimonas, G.: 1993, 'Surface-Drag Instabilities in the Atmospheric Boundary Layer', *J. Atmos. Sci.* **50**, 1914–1924.
- Einaudi, F. and Finnigan, J. J.: 1993, 'Wave-Turbulence Dynamics in the Stably Stratified Boundary Layer', *J. Atmos. Sci.* **50**, 1841–1864.
- Jeffreys, H.: 1925, 'The Flow of Water in an Inclined Channel of Rectangular Section', *Phil. Mag.* **49**, 793–807.
- Lee, X.: 1997, 'Gravity Waves in a Boreal Forest: A Linear Analysis', *J. Atmos. Sci.* **54**, 2574–2585.
- Lee, X. and Barr, A. G.: 1998, 'Climatology of Gravity Waves in a Forest', *Quart. J. Roy. Meteorol. Soc.* **124**, 1403–1419.
- Lee, X., Neuman, H., Den Hartog, G., Feuntes, J., Black, T., Mickle, R., Yang, P., and Blanken, P.: 1997, 'Observation of Gravity Waves in a Boreal Forest', *Boundary-Layer Meteorol.* **84**, 383–398.
- Maslowe, S. A. and Thompson, J. M.: 1971, 'Stability of a Stratified Free Shear Layer', *Phys. Fluids* **14**, 453–458.
- Miles, J. W. and Howard, L. N.: 1964, 'Note on a Heterogeneous Shear Flow', *J. Fluid Mech.* **20**, 331–336.
- Raupach, M. R., Finnigan, J. J., and Brunet, Y.: 1996, 'Coherent Eddies and Turbulence in Vegetation Canopies: The Mixing-Layer Analogy', *Boundary-Layer Meteorol.* **78**, 351–382.